Tridentate acylhydrazone copper(II) complexes with heterocyclic bases as coligands. Synthesis, spectroscopic studies, crystal structure and cytotoxicity assays

Yacelis Burgos-López[a], Lucia M. Balsa[a], Oscar E. Piro[b], Ignacio E. León[a], Javier García-Tojal[c], Gustavo A. Echeverría[b], Ana C. González-Baró[a], Beatriz S. Parajón-Costa[a*]

[a] CEQUINOR (CONICET, CCT-La Plata, UNLP), Bvd. 120 N°1465, B1900AVV- La Plata, República Argentina. [a*] beatrizp @ química.unlp.edu.ar

[b] Departamento de Física, Facultad de Ciencias Exactas, Universidad Nacional de La Plata and IFLP (CONICET, CCT-La Plata), C.C. 67, B1900AVV - La Plata, República Argentina

[c] Departamento de Química, Universidad de Burgos, Pza. Misael Bañuelos s/n, E-09001 Burgos, España.

ABSTRACT

Two new penta-coordinated copper(II) hydrazone coordination compounds with 2,2′ bipyridine **(I)** or 1,10 phenatroline **(II)** as coligands are synthesized and characterized in the solid state and in solution by spectroscopic methods (FTIR, Raman, UV-vis, EPR). Single crystal X-ray studies show that they have closely related molecular structures with the copper center in a distorted square pyramidal O_2N_3 environment. The N-acylhydrazone, 4-hydroxy-N′-[(E)2-hydroxy-3-methoxybenzylidene]benzohydrazide, H_2L, coordinates tridentate through its ONO donor atoms as monoanion (HL^-) in the cationic complex **(I)**, [Cu(HL)(bipy)](NO_3). During the period that takes the synthesis reaction of compound **(II)**, [Cu(L)(*o*-phen)] to complete, keto-amine to enol-imine tautomerization of H_2L occurs and the hydrazone coordinates as tridentate dianionic ligand (L^{2-}). The fivefold coordination sphere of the complexes is completed with the nitrogen atoms of the respective coligands. Cytotoxicity studies against bone (MG-63, $IC_{50(I)} = 5.6 \pm 1.0$, $IC_{50(II)} = 3.5 \pm 0.3$), breast (MCF-7, $IC_{50(I)} = 10.8 \pm 1.9$, $IC_{50(II)} = 4.0 \pm 1.3$), (MDA-MB-231, $IC_{50(I)} = 11.4 \pm 0.6$, $IC_{50(II)} = 5.3 \pm 0.2$) and lung cancer cells (A549, $IC_{50(I)} = 7.7 \pm 0.7$, $IC_{50(II)} = 7.0 \pm 0.4$) reveals increased effectiveness of both complexes compared with the free ligand, the copper nitrate salt and the reference metallodrug cisplatin (CDDP).

Keywords: Cu(II)-complexes; Hydrazones; N,N heterocycles; Spectroscopy; Crystal structure; Anticancer activity.

1. INTRODUCTION

Copper is an essential trace element for all living organisms and one of the most predominant in the human body where it is found in the oxidation states +1 and +2. It participates in a wide variety of physiological processes as component of many metalloproteins and enzymes, being involved in catalytic processes and in various molecular interactions.[1-3] Copper can also be toxic and, in this sense, some human health disorders and diseases are related with high level of this metal in the body.[1,2]

In the field of coordination chemistry, copper-based compounds have been investigated by their role as enzyme inhibitors and by their therapeutic potential as antiviral, antibacterial, antiparasitic and antiinflamatory agents.[2-4] The discovery of the chemical nuclease activity of the $[Cu(\textit{o}\text{-phen})_2]^{+}$[5] has also led to the development of many copper complexes explored as a new generation of potential anticancer drugs with lower toxic effects and drug resistance to the chemotherapy than platinum-based compounds.[2,4-8] Among them, ternary copper complexes containing polydentate ligands and N,N heterocyclic bases, such as 1,10 phenanthroline *(o*-phen), 2,2′-bipyridine (bipy) and their derivatives, have been tested against different tumour panel cell lines showing a promising effectiveness as chemotherapeutics for cancer therapy.[6-11] In many cases, the anticancer activity of the copper compounds was attributed either to a strong interaction with the DNA molecule through surface associations or intercalation, or to a potential DNA cleavage through hydrolytic or oxidative mechanisms.[6-12] In other cases, it was ascribed to the antiangiogenic, antimetastatic or anti-inflammatory properties of the complexes.[13] Particularly, aroyl- and acyl-hydrazones are an important family of compounds among the polydentate ligands that form stable complexes with copper. They are of growing interest, not only in chemistry and physics but also in biochemistry and medicine, because of their multiple applications. From the medicinal point of view, their therapeutic properties as antimicrobial, antifungal, antiviral, antitumor, anticonvulsant, agents were investigated and reported some years ago.[14-16] On the other hand, the structural characteristics of the hydrazones, their flexibility and capacity to chelate transition metals become them attractive materials for the design of new coordination compounds of relevance because of their bio and physicochemical properties.[17-20] Hydrazones and their metal complexes have also found applications in the field of supramolecular chemistry and no-linear optics[21] and as sensors, molecular photo-switches and catalyst.[22-24]

In a previous work we reported the synthesis, physicochemical characterization and DFT study of a new acyl hydrazone copper complex of formula $[Cu(HL)(OH_2)_2](NO_3)$, named complex **(1)**, hereafter.[25] The 4-hydroxy-N′-[(E) 2-hydroxy-3-methoxybenzylidene] benzohydrazide] ligand (H_2L) coordinates to the copper ion as monoanion (HL^-) through the phenolate oxygen, the azomethine nitrogen and the carbonyl oxygen atoms, in the keto-amine tautomeric form (A), (Scheme 1). The anticancer activity of **(1)**, on leukemia, lung, bone and breast cancer cells, was evaluated and reported together with the physicochemical characterization. The complex showed cytotoxic effectiveness on all cancer cell lines tested, with IC_{50} values in the 5-12 μM range. [25] These values are in the order of those determined for many copper complexes which showed higher anticancer activity than cisplatin (CDDP). [6,8,17]

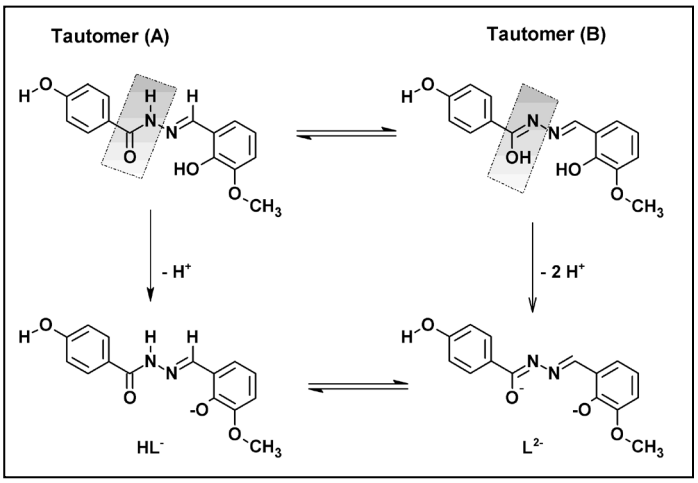

Scheme 1. Tautomeric equilibrium of the hydrazone ligand H_2L. The hydrazide fragment adopts the keto-amino (amido) form in the tautomer A, and the enol-imino (iminol) form in the tautomer B. The corresponding monoanion (HL^-) and dianion (L^{2-}) are also shown.

In the present work we describe the synthesis and the physicochemical characterization, by single crystal X-ray diffraction methods (XRD) and spectroscopic techniques in the solid state and in solution, of two new ternary copper complexes, obtained by interaction of compound **(1)** with 2,2′ bipyridine or 1,10 phenanthroline. In the new compounds of stoichiometry $[Cu(HL)(bipy)](NO_3)$ **(I)** and [Cu(L)(*o*-phen)] **(II)**, the N,N chelating bases replaces the water molecules in the coordination sphere of the parent compound **(1)** and the hydrazone, H_2L, adopts the keto-amino or the enol-imino tautomeric form (Scheme 1), coordinating as monoanion in **(I)** or as di-anion in **(II)**.

Finally, considering the anticancer activity shown by the precursor compound (**1**) and other

Cu(II) complexes with different ligands[6-11], we have evaluated the cytotoxicity as antitumoral of the ternary copper complexes against MG-63 (human osteosarcoma), MCF7 (breast adenocarcinoma), MDA-MB-231 (triple negative breast adenocarcinoma), A549 (lung adenocarcinoma) cancer cell lines and the results are herein also discussed.

2. EXPERIMENTAL

2.1. Materials and Methods

All reagents and solvents were of analytical grade. 2-hydroxy-3-methoxybenzaldehyde (*o*-vanillin) and 4-hydroxybenzhydrazide (Sigma), $Cu(NO_3)_2 \cdot 2.5H_2O$ (Riedel de Haën), 2,2′ bipyridine and 1,10 phenantroline (Aldrich), methanol (MeOH, Carlo Erba), absolute ethanol (EtOH, Emsure), 96% ethanol (EtOH, PuroCol) and dimethylsulfoxide (DMSO, Merck) were used as acquired without further purification. Tissue culture materials were purchased from Corning (Princeton, NJ, USA), Dulbecco's modified Eagle's medium (DMEM) and TrypLE ™ were obtained from Gibco (Gaithersburg, MD, USA) and fetal bovine serum (FBS) was purchased from Internegocios (Argentina). All the cell lines were purchased from ATCC (American Type Culture Collection).

2.2. General Procedure for Synthesis

The $[Cu(HL)(OH_2)_2](NO_3)$ compound **(1)** and the hydrazone ligand (H_2L) used as starting materials were synthetized according to the methodology previously reported.[25, 26]

The $[Cu(HL)(bipy)](NO_3)$ **(I)** and [Cu(L)(o-Phen)]**(II)** complexes were prepared according to the following procedure: 0.25 mmol of 2,2 bipyridine (0.03905 g) or 1,10 phenanthroline (0.0451g) respectively dissolved in 20 ml of methanol were dropwise added to a 10 ml methanol solution containing 0.25 mmol (0.1117 g) of the parent compound **(1)**. The mixtures were refluxed for 9 hours, until bright deep green solutions were obtained. Afterwards, they were let to reach room temperature and green single crystals suitable for X-ray structural analysis of **(I)** and **(II)** were obtained after one week and two months, respectively. They were isolated by filtration and stored in a desiccator. The yield was 43% (0.0604g) for (**I**)) and 24% (0.0313g) for **(II)**. The purity of the compounds was verified through elemental chemical analysis: complex **(I):** Calc. for $C_{25}H_{21}N_5O_7Cu$: C, 61.42%; H, 3.82 %; N, 10.61%; Found: C, 61.58 %; H, 3.93 %; N, 10.72%; complex **(II)**: Calc. for $C_{27}H_{20}N_4O_4Cu$: C, 52.96 %; H, 3.73 %; N, 12.35%; Found: C, 52.99 %; H, 3.80%; N, 12.42%.

2.3. Physicochemical Methods

Elemental chemical analysis (C, H, N) of the complexes were performed with an Exceter CE 440 analyser. FTIR spectra were measured in the 4000-400 cm^{-1} range with a FTIR Bruker EQUINOX 55 instrument using the KBr pellet technique. Raman spectra were obtained with AWITEC alpha 300 RA spectrophotometer, using laser excitation wavelength of 532 nm and a 20x and 50x objective lenses for complex **(I)** and **(II),** respectively. Electronic spectra were recorded in the 260-900 nm spectral range in freshly prepared solution of the compounds in DMSO with a Shimatzu UV-2006 spectrophotometer, using 10 mm quartz cells. Stability in DMSO was determined recording the spectra at room temperature at various time intervals for 72 hours, in the same spectral range.

The X-ray diffraction experiments were performed on an Oxford Xcalibur, Eos, Gemini CCD diffractometer, employing graphite-monochromated MoKα (λ = 0.71073 Å) radiation. X-ray diffraction intensities were collected (ω scans with ϑ and κ-offsets), integrated and scaled with CrysAlisPro [27] suite of programs. The unit cell parameters were obtained by least-squares refinement (based on the angular settings for all collected reflections with intensities larger than seven times the standard deviation of measurement errors) using CrysAlisPro. Data were corrected empirically for absorption with the multi-scan method implemented in CrysAlisPro.

The structures were solved by intrinsic phasing with SHELXT of the SHELX suit of programs [28] and refined with SHELXL of the same package. All hydrogen atoms were located in a difference Fourier map and, except the methyl and the hydroxyl ones of $[Cu(HL)(bipy)]NO_3$ (**I**), they were refined at their found positions with isotropic displacement parameters. The methyl and hydroxyl hydrogen atoms of **(I)** were refined with the riding model considering the $–CH_3$ and –OH as rigid groups allowed to rotate around the C-CH_3 and C-OH bonds, respectively, such as to maximize the residual electron density at the calculated H-positions. The imino H-atom was refined with N-H distance restrained to a target value of 0.86(1) Å. Crystal data, data collection procedure, structure determination methods and refinement results are summarized in Table 1.

X-band EPR spectra on powdered samples and frozen solutions were recorded in a Bruker EMX spectrometer, supplemented with a Bruker ER 036TM NMR-teslameter, an Agilent 53150A frequency counter and a Bruker ER 4131VT accessory for variable temperature experiments, which incorporated a liquid nitrogen evaporator, a heater and the BVT3000 temperature controller. Solution room-temperature studies were performed with a flat quartz cell, whereas the experiments at 120 K were carried out inside a quartz tube by quickly

freezing the solvents mixture by immersion in a liquid nitrogen-containing Dewar. SimFonia [29] and Kaleidagraph v4.1[30] programs were used for fitting the spectra and drawing the graphics, respectively. Experimental details are provided in the figure captions.

Table 1. Crystal data and structure refinement results for compounds **(I)** and **(II)**

Complex	[Cu(HL)(bipy)](NO$_3$) (I)	Cu(L)(*o*-phen) (II)
Chemical formula	$C_{25}H_{21}N_5O_7Cu$	$C_{27}H_{20}N_4O_4Cu$
Formula weight	567.01	528.01
Temperature (K)	293(2)	293(2)
Wavelength (Å)	0.71073	0.71073
Crystal system	Monoclinic	Monoclinic
Space group	P 2_1/n	P 2_1/c
Unit cell dimensions:		
a(Å)	9.9289(3)	7.2388(3)
b(Å)	13.3081(4)	19.544(1)
c(Å)	19.2427(7)	16.0451(6)
β(º)	100.352(4)	93.149(4)
Volume (Å^3)	2501.2(1)	2266.6(2)
Z	4	4
Density (calculated, Mg/m^3)	1.506	1.547
Absorption coeff. (mm^{-1})	0.929	1.008
F(000)	1164	1084
Crystal color	Green	Green
Crystal size (mm^3)	0.094 x 0.129 x 0.190	0.021 x 0.097 x 0.117
ϑ-range (º) for data collection	2.942 to 28.880	3.005 to 29.216
Index ranges	-13≤h≤13, -18≤k≤16, -23≤l≤25	-9≤h≤9, -26≤k≤25, -22≤l≤11
Reflections collected	12200	11578
Independent reflections	5426 [R(int) = 0.0339]	4969 [R(int) = 0.0677]
Obs. reflections [I>2σ(I)]	3671	2941
Completeness (%)	99.8 (to ϑ = 25.242°)	99.8 (to ϑ = 25.242°)
Refinement method	Full-matrix least-squares on F^2	Full-matrix least-squares on F^2
Data / restraints / parameters	5426 / 1 / 413	4969 / 0 / 394
Goodness-of-fit on F2	1.007	1.028
Final R indices[a] [I>2σ(I)]	R1 = 0.0545, wR2 = 0.1157	R1 = 0.0610, wR2 = 0.0783
R indices (all data)	R1 = 0.0906, wR2 = 0.1352	R1 = 0.1269, wR2 = 0.0963
Larg. diff. peak / hole (e.Å^{-3})	0.659 / -0.689	0.373 / -0.454

[a]$R1=\Sigma||F_o|-|F_c||/\Sigma|F_o|$, $wR2=[\Sigma w(|F_o|^2-|F_c|^2)^2/\Sigma w(|F_o|^2)^2]^{1/2}$

2.4. Cell line and growth conditions

MG-63 (bone), A549 (lung), MCF-7 (breast) cancer cells were grown in DMEM containing 10 % FBS, 100 U/mL penicillin, and 100 µg/mL streptomycin at 37° C in a 5 % CO_2 atmosphere whilst MDA-MB-231 (breast) were grown in F12-DMEM. Cells were seeded in a 75-cm^2 flask, and when 70–80 % of confluence was reached, cells were subcultured using 1 mL of TrypLE ™ per 25-cm^2 flask. For experiments, cells were grown in multiwell plates. When cells reached the desired confluence, the monolayers were washed with PBS and were incubated under different conditions according to the experiments.

2.5. Cell viability study: 3-(4,5-Dimethylthiazol-2-yl)-2,5-diphenyltetrazolium bromide assay

The 3-(4,5-dimethylthiazol-2-yl)-2,5-diphenyltetrazolium bromide (MTT) assay was performed according to Mosmann.[31] Briefly, cells were seeded in a 96-well dish for 24 h and treated with different concentrations (1-50 μM) of the compounds **(I)** and **(II)** at 37° C for 24 h. Then, the medium was changed, and the cells were incubated with 0.5 mg/mL MTT under normal culture conditions for 3 h. Cell viability was marked by the conversion of the tetrazolium salt MTT to a colored formazan by mitochondrial dehydrogenases. Color development was measured spectrophotometrically with a microplate reader (model 7530, Cambridge Technology, USA) at 570 nm after cell lysis in DMSO (100 μL per well).

3. RESULTS AND DISCUSSION

3.1. Crystal structures of [Cu(HL)(bipy)](NO_3) (I) and [Cu(L)(*o*-phen)] (II):

ORTEP[32] plots of complexes **(I)** and **(II)** are shown in Figures 1 and 2, respectively, and corresponding bond distances and angles around the Cu(II) ion are compared in Table 2. A complete list of experimental geometrical parameters is available in Tables S1-S4 a and b (ESI). Crystallographic data show that in $[Cu(HL)(bipy)]^+$ the hydrazone is coordinated to the copper ion as in the parent compound **(1)**, acting as monoanion (HL^-) by deprotonation of the OH group of the *o*-vanillin fragment (Figure 1). In the neutral [Cu(L)(*o*-phen)] complex, the hydrazone interacts as L^{2-} (Scheme 1) by further deprotonation of the N2 nitrogen atom with enolization of the amide functionality, as is shown in Figure 2.

Despite the different charge on the hydrazone and the nature of the N,N heterocycles completing the coordination environment of the metal, the complexes exhibit closely related molecular structures with the Cu(II) ion in a distorted square pyramidal (SP) environment. The complexes crystallize with the copper ion coordinated at the pyramid basis to a nearly planar hydrazone, functioning as a tridentate ligand through the deprotonated phenolic oxygen atom [Cu-O1 distances of 1.906(2) Å for **(I)** and 1.931(2) Å for **(II)**], the azomethine nitrogen atom [Cu-N1 distances of 1.925(3) Å for **(I)** and 1.922(3) Å for **(II)**] and the carbonyl O-atom [Cu-O2 distances of 2.015(2) Å for **(I)** and 1.980(3) Å for **(II)**] with the metal located close onto the coordination plane. The distorted square basis is completed with one N-atom of the bipy ligand in **(I)** [d(Cu-N4) = 2.019(3) Å] and of *o*-phen ligand in **(II)** [d(Cu-N4) = 2.013(3) Å]. The pyramid apex is occupied by the other nitrogen atom of the heterocycles at longer distances [d(Cu-N3) = 2.240(3) Å for **(I)** and 2.264(3) Å for **(II)**],

consistent with the second order Jahn-Teller effect for penta-coordinated Cu(II) complexes along the apical axis.[12,33-35] This geometry is also in accordance with the calculated Addison parameter[36] , employed to describe five-coordinated complexes. The parameter is defined as $\tau = (\beta-\alpha)/60$, where β and α are the two largest angles of the polyhedron. Thus, the extreme values, 0.0 and 1.0, are expected for perfect square pyramid or trigonal bipyramid, respectively. In both complexes, the calculated parameter was close to 0.0: 0.18 for **(I)** [β = 171.49°(10), α = 160.65°(12)] and 0.12 for **(II)** [β = 172.21°(14), α = 165.12°(11)].

A five member chelate ring is also formed by the interaction of the nitrogen donor atoms of the bypy (Cu-N4-C21-C20-N3) or *o*-phen (Cu-N4-C26-C27-N3) bases with the metal centre. The coordination of the ligand, as HL^- or L^{2-}, to the copper ion originates two quasi-rings of five and six members, that share the Cu-N1 bond, as can be seen in the Figures 1 and 2.

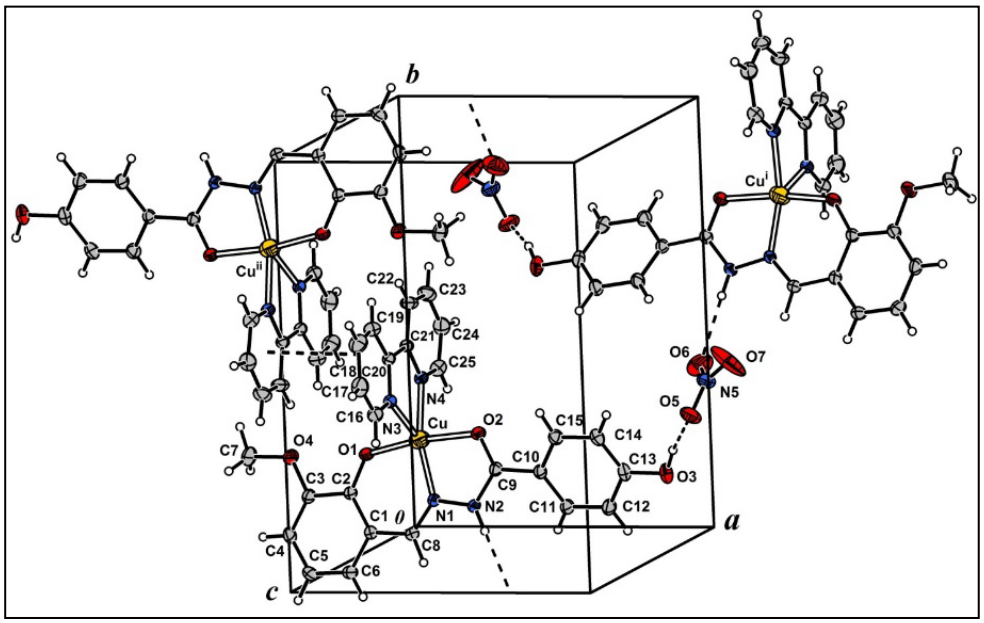

Figure 1. View of [Cu(HL)(bipy)](NO$_3$) down the crystal *c*-axis showing the labels of the non-H atoms and their displacement ellipsoids of non-H atoms at the 30% probability level. Copper-ligand interactions are indicated by open bonds and H-bond and π-π interactions by dashed lines. The upper right and left complexes are respectively related to the fully labelled one through the two-fold screw-axis symmetry operation (i) 3/2-x, 1/2+y, 3/2-z and the inversion symmetry operation (ii) –x, 1-y, 1-z.

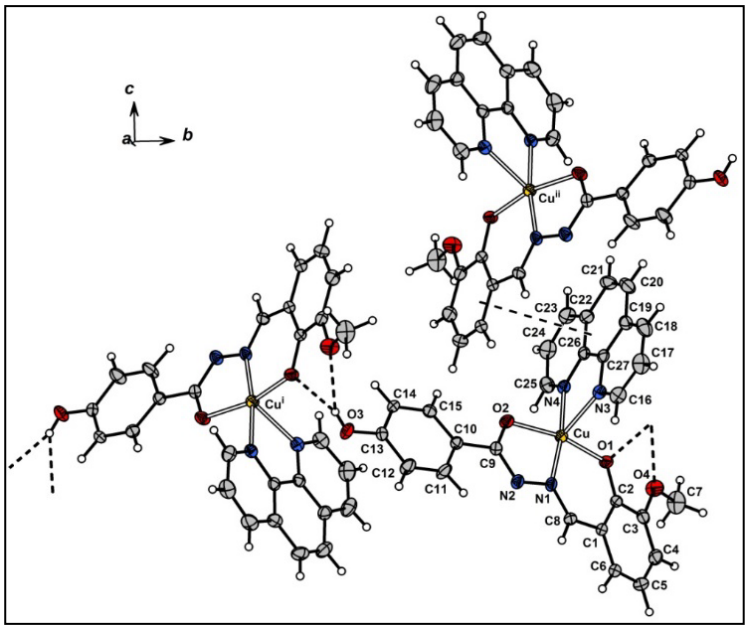

Figure 2. View of [Cu(L)(*o*-phen)] down the crystal *a*-axis. The complex on the left and the one at the upper right are respectively related to the labelled complex by the two-fold screw-axis symmetry operation (i) 1-x, -1/2+y, 3/2-z and the glide plane symmetry operation (ii) x, 3/2-y, 1/2+z.

The molecular structure and metrics of $[Cu(HL)(bipy)]^+$ complex are closely related to the ones reported for the nitrate salts of $[Cu(HL)(OH_2)_2]^+$ [25] and $[Cu(HL)(CH_3OH)_2]^+$ [35] complexes. Bond distances and angles within the HL^- and L^{2-} ligands are also in general agreement with the corresponding values reported for the solid state neutral H_2L. As expected, the major changes occur at the groups involved in the binding to the metal (see Table 2). In fact, due to the coordination with the copper ion, the phenolate C-O1 bond length shortens from d(C-O1H) = 1.352(6) Å in H_2L to d(C-O1) = 1.307(4) Å for **(I)** and 1.322(4) Å for **(II)**. When comparing **(II)** with the neutral ligand, the formally (O)C9-N2(H) single bond of the (O)C9-N2(H)-N1=C(H)- group shortens in 0.01 Å because of the deprotonation at N2 and coordination of N1 to the metal ion. Likewise, in both complexes the carbonyl (C9=O2) bond lengthens in a degree that depends on the strength of the metal-oxygen bond [+0.008 Å for **(I)** and +0.045 Å for **(II)**]. The highest increase in the (C-O) single bond character of this group in **(II)** is consequence of the deprotonation of N2 and binding to the metal through the deprotonated oxygen of the enolized ($C9\text{-}O2^-$) function.[37]

The data also show that the (C9-N2) and (C9=O2) bond distances of **(I)** agree with those found in the parent compound **(1)**[25] and in other complexes where the hydrazone is coordinated as monoanion, in the keto-amine tautomeric form (A) (Scheme 1).[17,37,38] For complex **(II)** these bond distances are close to the values reported for C-O(H) (1.29-1.31 Å)

and C=N (1.28-1.32 A°) for hydrazones that bind to the metal ion as L^{2-}, in the tautomeric enol-imine form (B) (Scheme 1).[37-39]

Table 2. Bond distances [Å] and angles [°] around metal in **(I)** and **(II)**

Bond distances	H_2L	(I)	(II)	Bond angles	(I)	(II)
C2-O1	1.352 (6)	1.307 (4)	1.322 (4)	O1-Cu-N1	92.0 (1)	93.1(1)
C8-N1	1.279 (6)	1.287 (4)	1.288 (4)	O1-Cu-O2	171.5 (1)	165.1 (1)
N1-N2	1.385 (6)	1.386(4)	1.388(4)	N1-Cu-O2	80.3(1)	80.4(1)
C9-N2	1.328 (6)	1.333(4)	1.319(4)	O1-Cu-N4	94.7(1)	90.9(1)
C9-O2	1.240 (6)	1.248 (4)	1.285 (4)	N1-Cu-N4	160.7(1)	172.2(1)
Cu-N1		1.925 (3)	1.922 (3)	O2-Cu-N4	91.7 (1)	94.2 (1)
Cu-O1		1.906 (2)	1.931 (2)	O1-Cu-N3	97.3 (1)	97.6 (1)
Cu-O2		2.015 (2)	1.980 (3)	N1-Cu-N3	120.2 (1)	108.0 (1)
Cu-N3		2.240(3)	2.264(3)	O2-Cu-N3	89.6 (1)	97.1 (1)
Cu-N4		2.019(3)	2.013(3)	N4-Cu-N3	77.9 (1)	78.1 (1)

In both crystal lattices, neighbouring complexes are related by a crystallographic two-fold screw axis and linked to each other through H-bonds giving rise to a chain structure that extends along the crystal *b*-axis (see Figures 1 and 2). In **(I)**, the nitrate ions serve as O···ONO_2···HN bridges where the nitrate oxygen atoms act as acceptor of OH···ONO_2 and NH···ONO_2 bonds [d(O···ONO_2) = 2.709(5) Å and d(N···ONO_2) = 3.096(6) Å]. In **(II)**, the complexes are H-bonded to each other through bifurcated OH···O links, the strongest one involving as acceptor the phenoxo oxygen (O1) and the weaker one the methoxy oxygen (O4) [OH···O bond distances of 2.697(4) and 3.102(4) Å]. The H-bonding structure of both compounds is further detailed in Tables S5 a and b (ESI).

Neighbouring (inversion-related) H-bonded chains in **(I)** are arranged with the planar bipy rings 3.445(4) Å apart and strongly overlapped with each other (see Figure 1), hence suggesting inter-chain π-π interaction. The shortest inter-chain Cu-Cu distance is 7.4819(8) Å, much lesser than the observed intra-chain Cu-Cu distance of 14.0209(9) Å.

Neighbouring (glide mirror-related) H-bonded chains in **(II)** are arranged with the ring of the aldehyde fragment on a chain nearly parallel (at about 3.41 A) and partially overlapped to the planar (*o*-phen) ring of the adjacent chain (see Figure 2), hence suggesting appreciable inter-chain π-π interaction. The shortest Cu-Cu distance between chains is 8.0716(3) Å and within a chain is equal to 10.3813(6) Å. In both complexes, H-bond and π-π interactions could provide electronic paths for super-exchange coupling between unpaired electrons on neighbouring metals in the lattices. This is discussed in the following section.

3.2. EPR spectroscopy

Figures 3 and Figure 4 depict the EPR spectra of powdered **(I)** and **(II)** compounds at temperatures ranging from RT to 120 K. Compound **(I)** exhibits a rhombic-spectrum at 298 K whose intensity increases, as expected, on lowering the temperature (200 K) and undergoes a drastic broadening at 120 K (Figure 3).

The best fit for the experimental data at each temperature gives the following *g*-values: g_x = 2.058, g_y = 2.085 and g_z = 2.258, at 298 K; and g_x = 2.038, g_y = 2.076 and g_z = 2.286 at 120 K (see Figure S1 of ESI, note that the band widths in the XY plane at 120 K, H_x and H_y, are about three times broader than those at 298 K). These features are characteristic of a $d_{x^2-y^2}$ ground-state, in good agreement with the square pyramidal geometry deduced from the crystallographic results (Addison parameter, τ = 0.18).[36]

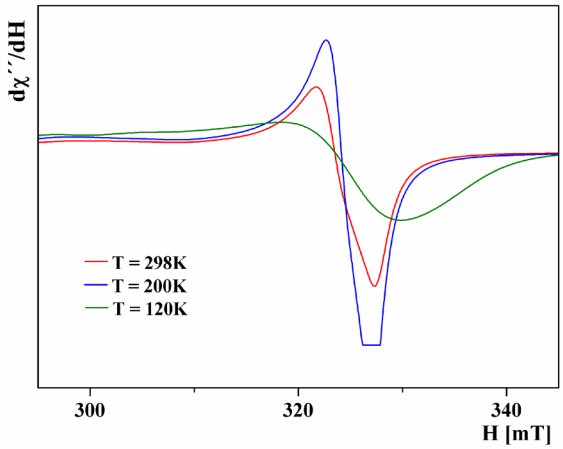

Figure 3. EPR spectra of complex **(I)** at different temperatures. Experimental details: modulation frequency = 100 kHz, modulation amplitude = 0.1 mT, time constant = 40.96 ms, conversion time = 81.92ms, gain = 6,3 x 10^3, power = 2.0 mW, microwave frequency = 9.4240 GHz.

At 298 K, the calculated *G* parameter ($G = g_{\parallel}$-2/$g_{\perp}$-2) is 3.6.[40,41] This value is within the 3.5-5.0 range, where the observed *g*-values are still considered meaningful, but it lies out of the 4.0-4.5 range, suggesting the presence of small magnetic coupling. On the other hand, at 120 K, the *G* parameter is 5.0, just in the limit of the magnetic coupling range. In fact, magnetic interactions between the monomeric paramagnetic species in the crystal structure could explain, at least in part, the broadening observed on lowering temperatures. Concerning this point, the shortest distance between Cu(II) ions is (Cu···Cu^i) = 7.4819(8) Å (where i = –x, 1-y, -z). Nevertheless, other possibilities are not discarded.

X-band EPR spectra of **(II)** in solid state do not show any noticeable changes with temperature (Figure 4). The shape regards an inverted axial spectrum, with g_1 = 2.1560, g_2 = 2.1170 and g_3 = 2.0565 (Figure S2 of ESI).

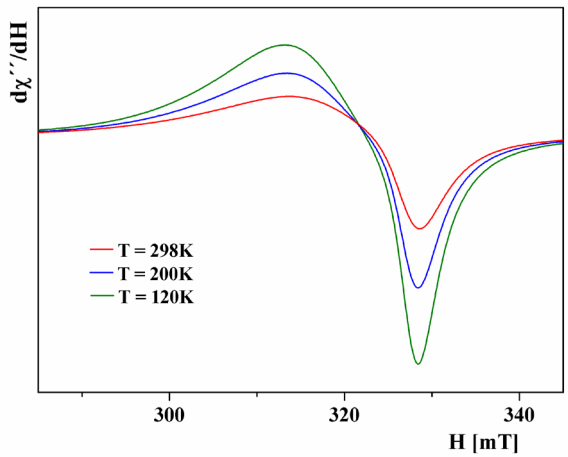

Figure 4: EPR spectra of **(II)** at different temperatures. Experimental details: modulation frequency = 100 kHz, modulation amplitude = 0.1 mT, time constant = 40.96 ms, conversion time = 81.92 ms, gain = 6,3 x 10^3, power = 2.0 mW, microwave frequency = 9.4257 (298 and 200 K) and 9.4270 GHz (120 K).

For this complex, the interpretation of the measurements is not straightforward, and different possibilities are open, as the presence of a d_z^2 ground state characteristic of trigonal bipyramidal geometry or differences in the alignment of the chromophores. In this sense, the calculated *G* parameter is 0.4, which strongly suggests that the presence of significant exchange coupling between closely arranged monomers could be misaligning the principal axes. Regarding this, note that π-π interactions between 1,10-phenanthroline and phenol moieties relate Cu(II) ions placed at 8.0716(3) Å (see Figure 2), whose ONO donor sets from the hydrazone ligand form planes with angles 75.91(7)º. Because of this, the EPR spectrum would not show the molecular *g*-tensors, but a rhombic tensor g_1^{ex}, g_2^{ex} and g_3^{ex}, arisen from the magnetic exchange.

The expressions given in Equations 1-4 can be applied to evaluate the existence of magnetic coupling between non-equivalent magnetic monomers with a $d_{x^2-y^2}$ ground state.[42,43]

$$cos\,2\,\alpha = \frac{g_1^{ex} - g_2^{ex}}{g_1^{ex} + g_2^{ex} - 2g_3^{ex}} \qquad \text{Equation 1}$$

$$(g_1^{ex})^2 = g_{||}{}^2\, cos^2\,\alpha + g_{\perp}{}^2\, sin^2\,\alpha \qquad \text{Equation 2}$$

$$(g_2^{ex})^2 = g_{||}{}^2\, sin^2\,\alpha + g_{\perp}{}^2\, cos^2\,\alpha \qquad \text{Equation 3}$$

$$g_3^{ex} = g_{\perp} \qquad \text{Equation 4}$$

The 2α angle is that formed by the tetragonal axis of magnetically non-equivalent paramagnetic centres. In this case, it is the angle between the two planes built from the basal donor atoms of the coupled square pyramidal monomers. The calculated value is 75.89º, in an excellent agreement with the crystallographic 2α (75.91º).

In the same way, the Equations yield $g_{\|}$ = 2.214 and $g_{\perp}$ = 2.056, which are close to the experimental parameters deduced from the spectrum at 120 K of a (1:3) (MeOH:DMF) solution of complex (**II**) with an approximate 5x10^{-4} M concentration (Figure S3, ESI). In this case, the best fit of the experimental data is $g_{\|}$ = 2.236; $A_{\|}$ = 17.8 mT (185.8 x 10^{-4} cm^{-1}); and $g_{\perp}$ = 2.052; $A_{\perp}$ = 1.5 mT (14.4 x 10^{-4} cm^{-1}). The features of the frozen solution spectrum ($g_{\|} > g_{\perp} > 2.0023$) are characteristic of a $d_{x^2-y^2}$ ground-state of a square pyramidal geometry, which suggests that the ground state is retained in solution in good agreement with the crystallographic results (Addison's parameter, τ = 0.12).[36] The *G*-value for the frozen solution measurements is 4.5, as expected for negligible magnetic interactions between monomers (Hathaway and Billing, 1970).[40] The $A_{\|}$ vs. $g_{\|}$ relationship[44,45] is consistent with that expected for a neutral Cu(II) complex with two nitrogen and two oxygen donor atoms, (2N2O), as the crystal structure ratifies.

3.3. Vibrational spectroscopy

FTIR and Raman spectra of solid samples of **(I)** and **(II)** were registered in the 4000-400 cm^{-1} spectral range and they are shown comparatively with those of the precursor compound **(1)** and the N,N heterocycles in Figure S4 and S5 of ESI. We have previously reported a vibrational and DFT study of H_2L and the parent complex **(1)** that helped in the current band assignment.[25] Some of the most characteristic bands between 1600-400 cm^{-1} are listed in Table 3 (for atom numbering see Figures 1 and 2).

The IR band due to the stretching of the N2H group of the free ligand [25] is shifted from 3190 cm^{-1} in complex **(1)** to 3120 cm^{-1} in **(I)** and it is missing in the spectrum of **(II)** in which the hydrazone coordinates as L^{2-}. The phenolic O1H bands are absent in the spectra of the complexes indicating deprotonation and coordination of the phenoxo group to the metal ion. The coordination of the azomethine nitrogen (N1) and the oxygen (O2) atom of the amide functionality originates a decrease of the C9=O2 and C8=N1 double bond character (Table 2) and, consequently, the corresponding stretching bands shift to lower wavenumbers in the complexes. In the IR spectrum of the free ligand the stretching modes of these groups give rise to a band at 1646 cm^{-1} and 1608 cm^{-1}, respectively, whereas in complex **(I)** only one very strong IR absorption at 1605 cm^{-1} (Ra: 1623 cm^{-1}) is observed. This behaviour is like

to that found in the parent compound **(1),** where according to the calculations both stretching modes are coupled, as can be seen in Table 3. Instead, in the IR spectrum of **(II)** the C9=O2 stretching band is absent and a new absorption, assigned to the ν(C-O2$^-$) mode of the enolate moiety, appears at 1376 cm^{-1}.[19,20,39] These findings, and the absence of the N2H band of the amide group support that the hydrazone coordinates to the metal in enol-imine form, in agreement with the crystallographic data. Therefore, the stretching of the C9=N2-N1=C8 group of the dianionic ligand (L2$^-$) is attributed to a strong IR and Raman bands observed at 1611 cm^{-1} and 1609 cm^{-1} respectively.

Table 3. Assignment of some characteristic IR and Raman bands (cm^{-1}) of **(I)** and **(II)**, in the 1600-400 cm^{-1}region. The parent compound **(1)** is also included for comparison.

Complex (1)[25]	Complex (I)		Complex (II)		Assignment
IR	IR	Ra	IR	Ra	
1603 s	1605 vs	1623 vs			νC8=N1 + νC9=O2 + ν_R^{OHVA}
			1611 vs	1609 vs	ν(C8=N1-N2=C9) + ν_R^{OHVA}
1543 m	1541 m	1546 m	1549 w	1551 m	$[\nu_R + \delta OH]^{HBH}$
1438 m	1441 m-s	1442 vs	1441 m-s	1434 m	ν_{QR} (CuO1C2C1C8N1)
1384 s,b	1384 s,b				ν_{as} (NO_3^-)
		1358 m	1358 m	1355 sh	$\nu_{QR}^{Bipy/Phen}$
			1376 m		νC9-O2
1322 m, b	1329 m	1327 s			δN2H + ν_{as} (C10-C9-N2)
			1343 m	1344 m,w	νC2-O1 + ν_{as} (C10-C9=N2)
1312 sh	1322 sh	1318 sh			νC2-O1
1218 s	1218 s	1225 vw	1214 m	1218 vw	νN2-N1 + νC10C9
747 m	734 m-w		727 m	733 vw	δ_R^{OHVA} + δ_{QR}(CuO1C2C1C8N1)
577 vw	544 vw	547 w	550 vw		ν_s (N1-Cu-O1)
506 vw	489 vw	497vw	480 vw		νCuN1 + δ_{QR}(CuO1C2C1C8N1)
430 vw	415 vw	421vw	424 vw	422 vw	νCuO2

***References**:* OHVA: *o*-vanillin fragment; HBH: hydrazide fragment; R: ring; QR: quasi ring; ν: stretching; δ: in-plane deformation; γ: out-of-plane deformation. ***Intensity*:** vs: very strong, s: strong, m: medium, w- weak, vw: very weak, b: broad, sh: shoulder.

Upon complexation, the N2-N1 stretching band of H_2L at 1186 cm^{-1}, shifts approximately 30 cm^{-1} to higher wavenumbers in both compounds. In similar compounds, this shifting is attributed to a decrease in the repulsion forces between the lone electron pairs of the adjacent nitrogen atoms as a result of the coordination of N1 to the metal.[46] The intense and broad signal at 1384 cm^{-1} in the IR spectrum of complex **(I)**, that is not observed for **(II)**, is a characteristic band of the nitrate counterion.[47,48]

On the other hand, in the spectra of both complexes and similarly to that found previously for complex **(1),** new absorption bands are detected around 1400 cm^{-1} and below 700 cm^{-1},

which correspond to the stretching and in-plane deformational modes of the pseudo-rings originated by the coordination of H_2L to the metal.[25] Likewise, the new signals around 1350 cm^{-1} in both complexes are attributed to the stretching of the [CuN3CCN4] pseudo-rings formed by the coordination of the bipy or *o*-phen bases to the Cu(II) ion. Moreover, several ring bands of the heterocycles show changes of intensity after coordination and some of them frequency shifts. The strong IR bands due to the C=N stretching coupled with the C-H in-plane deformation mode at 1454 cm^{-1} (bipy) and 1422 cm^{-1} (*o*-phen) shift to 1469 cm^{-1} and 1427 cm^{-1}, in the spectrum of the respective complex. The bands observed between 850-700 cm^{-1}; assigned to the hydrogen out-of-plane bending modes of the heterocycles, shift slightly to lower wavenumbers.[49,50] In addition, weak IR bands below 550 cm^{-1}, absent in the spectrum of the free hydrazone, are assigned to the stretching vibrations of the ligand-to metal bonds.

3.4. Electronic spectroscopy

The electronic absorption spectra of the complexes, recorded for $2.5x10^{-5}$M DMSO solutions in the 260-900 nm spectral range, are shown in Figure 5 a and b, comparatively with that of the complex **(1).**

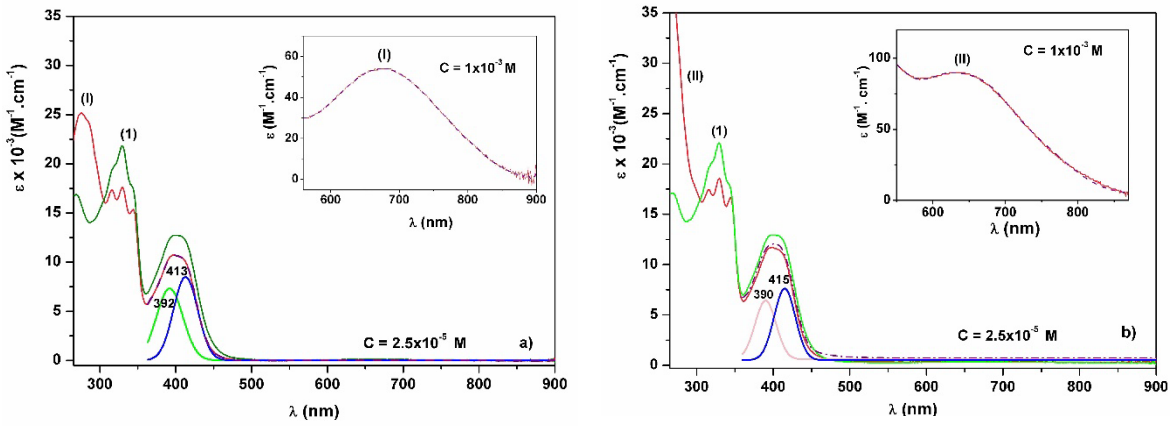

Figure 5. Electronic absorption spectra of complex **(I)** (a) and complex **(II)** (b) are shown comparatively with the spectrum of **(1).** The inset of the figures shows the corresponding d-d transitions.

The d-d transitions of the compounds are observed as broad bands in the 550-900 nm region (insets of the figures). These bands with low extinction coefficient values are centred at 684 nm for **(I)** and 641 nm for **(II)** and are consistent with a distorted square pyramidal geometry around the copper ion in the DMSO solution.[46,51,52] By comparison with our previous studies and considering the extinction coefficient, (ε), the absorptions maxima at 276 nm, 316 nm for complex **(I)** and at 266 nm, 315 nm for **(II)** are assigned to ligand-to-metal charge

transfer transitions (LMCT)[25] whereas the shoulders at 286 nm **(I)** and 278 nm **(II)** are a result of π→π* transitions of the coordinated heterocycles.[53]

The spectrum of H_2L shows absorptions with maxima at 300, 314 and 339 nm that shift towards lower energies upon coordination to the metal. Thus, the bands at 329 and at 344 nm for both complexes, which are like those previously observed for complex **(1)**, at 329 and 342 nm**,** are assigned to the hydrazone intraligand transitions.[25] The broad band centred at approximately 400 nm contains two components that were determined by deconvolution. The first one, at about 390 nm, corresponds to an intraligand transition of the hydrazone fragment (at 339 nm in the free ligand) and the second one, at 413 nn **(I)** and 415 nm **(II)**, may be originated by a combination of O→Cu and N→Cu charge transfer transitions. [46,51] On the other hand, both compounds are stable during 72 h in DMSO solution according to sequential measurements performed at room temperature.

3.5- Cytotoxicity Studies.

Cytotoxicity studies, evaluated by the MTT assay, were performed for complex **(I)** and **(II)** with four tumour cell lines: MG-63 (human osteosarcoma), MCF7 (breast adenocarcinoma), MDA-MB-231 (triple negative breast adenocarcinoma), A549 (lung adenocarcinoma). The cells were exposed to different concentrations, from 1 to 50 μM, of complexes **(I)** and **(II),** at 37°C for 24 h.

To establish the antitumor efficacy of both compounds their cytotoxic activities are compared with those of the clinical reference metal-based drug cisplatin (CDDP) on the tumour panel cell lines tested and the corresponding IC_{50} values are given in Table 4. The results indicate that both complexes are significantly more cytotoxic than cisplatin on all the cancer cells tested, mainly on those of lung (A549) and breast (MDA-MB-231) and they show a very good correlation with the IC_{50} values obtained with many copper complexes displaying an encouraging antitumor activity against different human cancer cell lines. [6,8,13,17,54] On the other hand, the IC_{50} values obtained with each complex reveal a considerable improvement of the cytotoxic activity compared with the free ligand and the copper ion, which cause an inhibitory effect only at high concentrations (IC_{50} > 100 μM, for the four cell lines tested).

Table 4. IC_{50} (μM) values of complex **(I)**, **(II)** and CDDP on the tumour panel cell lines tested after 24 h of incubation.

	IC_{50} ± SD

Cell lines	(I)	(II)	(CDDP)
MG-63	5.6 ± 1.0	3.5 ± 0.3	39 ± 2.0
MCF7	10.8 ± 1.9	4.0 ± 1.7	42 ± 2.7
MDA-MB-231	11.4 ± 0.6	5.3 ± 0.2	131 ± 2.5
A549	7.7 ± 0.7	7.0 ± 0.4	114 ± 2.0

It is noteworthy that the IC_{50} values of complex **(I)** and **(II)** on bone (MG-63) and lung cancer (A549) cells are lower than those previously obtained with the compound **(1)**, $[Cu(HL)(OH_2)_2]NO_3$[25], ($IC_{50(1)}$ = 8.8 ± 0.3 and $IC_{50(1)}$ = 12.0 ± 1.2, respectively) hence suggesting that the replacement of the coordination water molecules by an intercalator ligand, such as 2,2´bipyridine or 1,10-phenanthroline, improves the cytotoxicity of the compounds on both cancer cell lines.

Moreover, as it can be seen in Table 4, both complexes decrease cell viability on the cancer cells lines in the concentration range of 5-15 μM **(I)** and 2.5-10 μM **(II)**. These values reveal that the strongest antitumor effect is produced by the complex **(II)** and suggest that it is more bioactive than **(I)** against the four cancer cell lines tested.

4.- CONCLUSIONS

Two new mixed-ligand mononuclear copper complexes of 4-hydroxy-N´-[(E)2-hydroxy-3-methoxybenzylidene]benzohydrazide, containing 2,2 bipyridine or 1,10-phenantroline as co-ligands have been obtained and characterized by spectroscopic and X-ray diffraction techniques. The crystallographic and vibrational data (FTIR and Raman) show that the hydrazone ligand (H_2L) binds to the metal in the keto-amine tautomeric form in the complex **(I),** [Cu(HL)(bipy)](NO_3), and in the enol-imine form in the neutral compound **(II),** [Cu(L)(*o*-phen)]. The hydrazone interacts with the metal centre as mono-anion (HL^-) in **(I)** or as di-anion (L^{2-}) in **(II)**, coordinating in the pyramid base through its O,N,O donor atoms. The fivefold coordination is completed through the N,N atoms of the respective chelating ligands. The EPR data are consistent with a $d_{x^2-y^2}$ ground state for both complexes, in close agreement with the O_2N_3 distorted square pyramidal environment determined by XRD. Electronic spectra recorded several times during 72 h show that the compounds are stables during this period. The UV bands of the free hydrazone shift to lower energies upon coordination to the metal and new bands that correlates with intra-ligand transitions of the

heterocycles are identified. In the visible range, the d-d transitions are consistent with a distorted square pyramidal geometry in DMSO solution.

From the biologically point of view, the complexes are significantly more cytotoxic than the reference metallodrug cisplatin on the four-tumour cell tested, but mainly on lung (A549) and triple negative breast (MDA-MB-231) cancer cells. It is also important to highlight that the inclusion of the heterocycles on the copper coordination sphere improves the cytotoxicity of the compounds when compared with the $[Cu(HL)(OH_2)_2](NO_3)$ parent compound. Moreover, the IC_{50} values show that compound **(II)** exerts the strongest antitumor effect on the cancer lines tested appearing as a potential therapeutic agent with good prospects to be tested in forward specific assays.

Funding: This work was supported by CONICET (PIP 0651 and PIP 0340), UNLP (Grant 11/X673 and 11/041), ANPCyT (PICT 2016-1574) of Argentina and by Junta de Castilla y León and FEDER BU291P18 and BU049P20, Ministerio de Economía y Competitividad CTQ2016-75023-C2-1-P, Fundación Bancaria Caixa D. Etalvis I Pensions de Barcelona La Caixa-UBU001 and European Union H2020-LC-SC3-2020-NZE-RES-CC Nefertiti Project. O.E.P, I.E.L, G.A.E, A.G-B and B.P-C are members of the Researcher Career of CONICET. J.G-T is member of the Department of Chemistry (University of Burgos, Spain). YB-L and L.M.B are Fellows of CONICET.

Acknowledgments: The authors thank Dr. David Ibáñez Martinez (Department of Chemistry, University of Burgos, Spain) for Raman spectra.

Supplementary Information Available

Crystallographic structural data have been deposited at the Cambridge Crystallographic Data Centre (CCDC). Enquiries for data can be direct to Cambridge Crystallographic Data Centre, 12 Union Road, Cambridge, UK, CB2 1EZ or (e-mail) deposit@ccdc.cam.ac.uk or (fax) +44 (0) 1223 336033. Any request to the Cambridge Crystallographic Data Centre for this material should quote the full literature citation and the reference number CCDC 1577995 (**I**) and CCDC 1577994 (**II**).

Tables of fractional coordinates and equivalent isotropic displacement parameters of the non-H atoms (Tables S1a, S1b), full bond distances and angles (Tables S2a, S2b), atomic anisotropic displacement parameters (Tables S3a, S3b), hydrogen atoms positions (Tables S4a, S4b), H-bond distances and angles (Tables S5a, S5b). EPR spectra of powdered solid samples together with the best fits (Figure S1a, S1b and S2). EPR spectrum of complex (II)

in solution together with the best fit (Figure S3). FTIR and Raman spectra in the 3800 - 400 cm^{-1} range (Figure S4 and S5).

Conflict of interest

There are no conflicts of interest to declare.

References

[1] M.C Linder, M. Hazegh-Azam, Am. J. Clin. Nutr. 1996, 63, 797S–811S.

[2] I. Iakovidis, I. Delimaris and S.M. Piperakis, Mol. Biol. Int. 2011, 2011, 594529.

[3] C. Duncan, A.R. White, Metallomics 2012, 4, 127-138.

[4] M. Wehbe, A.W.Y. Leung, M.J. Abrams, C. Orvig, M.B. Ballya, Dalton Trans. 2017, 46, 10758-10773.

[5] D.S. Sigman, R. Landgraf, D.M. Perrin, L. Pearson, Metal Ions in Biological Systems, 1996, 33, 485-513.

[6] C. Santini, M. Pellei, V. Gandin, M. Porchia, F. Tisato, C. Marzano, Chem. Rev. 2014, 114 (1), 815−862.

[7] Z. Zhang, H. Wang, M. Yan, H. Wang, C. Zhang, Mol. Med. Rep. 2017, 15, 3-11.

[8] C. Marzano, M. Pellei, F. Tisato, C. Santini. Anti-Cancer Agents Med. Chem. 2009, 9 185-211, and references therein.

[9] D.A. Paixãoa, I.M. Marzano, E.H.L. Jaimes, M.Pivatto, D.L. Campos, F.R. Pavan, V.M. Deflond, P.I da S. Maiae, A.M. Da Costa Ferreira, I.A. Uehara, M.J.B. Silva, F.V. Botelho, E.C. Pereira-Maia, S. Guilardi, W. Guerra. J. Inorg. Biochem. 2017, 172, 138-146.

[10] M. Simunkova, P. Lauro, K. Jomova, L. Hudecova, M. Danko, S. Alwasel, I.M. Alhazza, S. Rajcaniova, Z. Kozovska, L. Kucerova, J. Moncol, L. Svorc, M. Valko**,** J. Inorg. Biochem. 2019, 194, 97-113.

[11] C. Rajarajeswari, M. Ganeshpandian, M. Palaniandavar, A. Riyasdeen, M.A. Akbarsha, J. Inorg. Biochem. 2014, 140, 255-268.

[12] S.Y. Ebrahimipour, I. Sheikhshoaie, M. Mohamadi, S. Suarez, R. Baggio, M. Khaleghi, M. Torkzadeh-Mahani, A. Mostafavi, Spectrochim. Acta, 2015, 142, 410-422.

[13] X. Shi, Z. Chen, Y. Wang, Z. Guo, X. Wang, Dalton Trans. 2018, 47, 5049-5054 and references therein.

[14] S. Rollas, Ş.G. Küçükgüzel, Molecules 2007,12, 1910-1939.

[15] J. Wahbed, S. Milkowski, SLAS Technol. 2019, 24, 161-168.

[16] Łukasz Popiołek, Med. Chem. Res. 2017, 26, 287-301.

[17] M.R. Rodríguez, L.M Balsa, O.E. Piro, G.A. Etcheverry, J. García-Tojal, R. Pis-Diez, I.E. León, B.S. Parajón-Costa, A.C. González-Baró, Inorganics 2021, 9(2), 9.
[18] K. Hu, G. Zhou, Z. Zhang, F. Li, J. Li, F. Liang, RSC Adv. 6 (2016) 36077-36084.
[19] V. Vrdoljak, G. Pavlović, N. Maltar-Strmećkic, M. Cindrić, New J. Chem. 2016, 40, 9263-9274.
[20] M. Cindrić, A. Bjelopetrović, G. Pavlović, V. Damjanović, J. Lovrić, D. Matković-Čalogović, Višnja Vrdoljak, New J. Chem. 2017, 41, 2425-2435.
[21] Q. Feng, Y. Li, G. Shi, L.Wang, W. Zhang, K. Li, H. Hou, Y. Song, J. Mater. Chem. C 2016, 4(36), 8552-8558.
[22] X. Su, I. Aprahamiam, Chem. Soc. Rev. 2014, 43, 1963-1981.
[23] D.J van Dijken, P. Kovaříček, S.P. Ihrig, S. Hecht, J. Am. Chem. Soc. 2015, 137, 14982-14991.
[24] A.G. Mahmoud, M.F.C. Guedes da Silva, K.T. Mahmudov, A.J.L. Pombeiro, Dalton Trans. 2019, 48, 1774-1785.
[25] Y. Burgos-López, J. Del Plá, L.M. Balsa, I.E. León, G.A. Echeverría, O.E. Piro, J. García-Tojal, R. Pis-Diez, A.C. González-Baró and B.S. Parajón-Costa, Inorg. Chim. Acta, 2019, 487, 31-40.
[26] J-F Lu, Acta Cryst. E64, 2008, o2032.
[27] CrysAlisPro, Oxford Diffraction Ltd., version 1.171.33.48 (release 15-09-2009 CrysAlis171.NET).
[28] G. M. Sheldrick, A short history of SHELX, Acta Crystallogr. A64, 2008, 112-122.
[29] WINEPR SimFonia v1.25, Bruker Analytische Messtecnik GmßH, 1996.
[30] Kaleidagraph v4.1.1 Synergy Software, 2010.
[31] T.T. Mosmann, J. Immunol. Methods 1983, 65, 55-63.
[32] L. J. Farrugia, ORTEP-3 for windows - a version of ORTEP-III with a graphical user interface (GUI), J. Appl. Crystallogr. 1997, 30, 565-566.
[33] S. Roy, P. Mitra, A. K. Patra, Inorg. Chim. Acta 2011, 370, 247-253 and references therein.
[34] R. Bikas, F. Ajormal, M. Emami, N. Noshiranzadeh, A. Kozakiewicz, Inorg. Chim. Acta, 2018, 478, 77-87.
[35] H. Hosseini-Monfared, E. Pousaneh, S. Sadighian, S.W. Ng, E.R.T. Tiekink, Z. Anorg. Allg. Chem. 2013, 639(2), 435-442.
[36] A.W. Addison, T.N. Rao, J. Reedijk, J. van Rijn, G.C.J. Verschoor, Chem. Soc. Dalton Trans. 1984, 1349-1356.

[37] A.A. Recio Despaigne, J.G. Da Silva, A. Cerúlia M. Do Carmo, O.E. Piro, E.E. Castellano, H. Beraldo, J. Mol. Struct. 2009, 920, 97-102.

[38] H. Hosseini-Monfared, H. Falakian, R. Bikas, P. Mayer, Inorg. Chim. Acta 2013, 394, 526-534.

[39] P.H.O. Santiago, M.B. Santiago, C.H.G. Martins, C.C. Gatto, Inorg.Chim.Acta 2020, 508, 119632

[40] B.J. Hathaway, D.E. Billing, Coord. Chem. Rev. 1970, 5, 143-207.

[41] B. J. Hathaway, D. E. Billing, J. Chem. Soc., Dalton Trans. 1972, 1196-1199.

[42] H. Abe, K. Ono, J. Phys Soc. Jpn. 1956, 11, 947-956.

[43] J. García-Tojal, A. García-Orad, J.L. Serra, J.L. Pizarro, L. Lezama, M.I. Arriortua, T. Rojo, J. Inorg. Biochem. 1999, 75, 45-54.

[44] J. Peisach, W.E. Blumberg, Arch. Biochem. Biophys. 1974, 165, 691-708.

[45] J.R. Pilbrow, *Transition ion electron paramagnetic resonance*, Oxford Science Publications, Oxford, 1990.

[46] S.T. Chew, K.M. Lo, S.K. Lee, M.P. Heng, W.Y. Teoh, K.S. Sim, K.W. Tan, Eur. J. Med. Chem. 2014, 76, 397-407.

[47] K. Nakamoto, *Infrared and Raman Spectra of Inorganic and Coordination Compounds*, *Sixth Edition*, J. Wiley & Sons, Inc., Hoboken, New Jersey, 2009.

[48] B.M. Gatehousse, E. Livingston, R.S. Nyholm, J. Chem. Soc. 1957, 4222-4225.

[49] A.A. Schilt, R.C. Taylor, J. Inorg. Nucl. Chem. 1959, 9, 211-221.

[50] J. S. Struel and J. L. Walter, Spectrochim. Acta 27A, 1971, 209-221.

[51] U. L. Kala, S. Suma, M. R. Prathapachandra Kurup, S. Krishnan, R. P. John, Polyhedron 2007, 26,1427-1435.

[52] A.B.P. Lever, *Inorganic Electronic Spectroscopy, 2da. Edition*, Elsevier Science Publishers B.V, Amsterdam, 1984.

[53] P. R. Reddy, A. Shilpa, N. Raju, P. Raghavaiah, J. Inorg. Biochem, 2011, 105, 1603-1612.

[54] O. Krasnovskaya, A. Naumov, D. Guk, P. Gorelkin, A. Erofeev, E. Beloglazkina, A. Majouga, Int. J. Mol. Sci. 2020, 21, 3965.